

GLAST Prospects for Swift-Era Afterglows

L. J. Gou¹ and P. Mészáros^{1,2}

ABSTRACT

We calculate the GeV spectra of GRB afterglows produced by inverse Compton scattering of the sub-MeV emission of these objects. We improve on earlier treatments by using refined afterglow parameters and new model developments motivated by recent Swift observations. We present time-dependent GeV spectra for standard, constant parameter models, as well as for models with energy injection and with time-varying parameters, for a range of burst parameters. We evaluate the limiting redshift to which such afterglows can be detected by the GLAST LAT, as well as AGILE.

Subject headings: gamma rays: bursts - radiation mechanisms: non-thermal

1. Introduction

GRB afterglow observations from X-rays to radio are generally well described by an external shock model (e.g. Mészáros 2006, for a recent review). However, model fits to the data still leave uncertainties in some of the parameters of the basic external shock model, and the bolometric luminosity depends on the poorly known GeV range spectrum. The Gamma Ray Large Area Space Telescope GLAST (McEnery & GLAST Mission Team 2006) is expected to be launched at the end of 2007. The Large Area Telescope (LAT) covers the energy range from 20 MeV to 300 GeV, while the Gamma Ray Burst Monitor (GBM) covers the range from 8 keV to 25 MeV. The effective area of the LAT is about 5 times larger than of the previous EGRET experiment at GeV energies. AGILE¹ was successfully launched on April 23, 2007, with an energy range of 30 MeV to 50 GeV (Tavani et al. 2006). It is hoped that the higher photon statistics at GeV energies of GLAST and AGILE will lead tighter

¹Department of Astronomy & Astrophysics, 525 Davey Laboratory, Pennsylvania State University, University Park, PA 16802

²Department of Physics, Pennsylvania State University, University Park, PA 16802

¹<http://agile.rm.iasf.cnr.it/index.html>

constraints on the burst parameters, and an improved understanding of the GeV afterglow spectra.

GLAST may also be able to test recent developments in the understanding of GRB afterglows, motivated by observations with the Swift satellite (e.g. Nousek et al. 2006; Zhang et al. 2006; Fox & Mészáros 2006; Zhang 2007). One such development is the presence of a shallow decay phase of the X-ray afterglow, which may be due to refreshed shocks or late energy injection (e.g. Zhang et al. 2006), or alternatively, it may be due to a change in time of the shock parameters (e.g. Ioka et al. 2006). We investigate here the effects of such new features on the expected GeV spectrum.

Another question of great interest is how far can GLAST detect the MeV to GeV emission from such bursts, both in the basic model and the case where new features such as the above are present. This requires a detailed calculation of the GeV spectrum as a function of time, with allowance for the changes in the dynamics implied by the injection, time variability, etc. The most conservative and widely considered mechanism for producing photons in this range is inverse Compton scattering (Panaitecu & Mészáros 1998; Totani 1998; Wei & Lu 1998; Chiang & Dermer 1999; Panaitecu & Kumar 2000; Sari & Esin 2001; Zhang & Mészáros 2001; Wang et al. 2001, 2006; Fan et al. 2007). Another potential mechanism is hadronic cascades following proton acceleration (Chiang & Dermer 1999; Zhang & Mészáros 2001; Fragile et al. 2004; Gupta & Zhang 2007). This mechanism is less well constrained, depending on the efficiency of proton acceleration; it may be important in the prompt phase, but its parameter regime is small and generally outside of the afterglow parameter fit range (Zhang & Mészáros 2001), so it is not considered here. The maximum distance to which GLAST could detect GRB afterglow was discussed by Zhang & Mészáros (2001) for the basic standard model, using a simplified analytical broken power law approximation to the IC spectrum. This resulted in an IC to synchrotron peak flux ratio which is overestimated by a factor ~ 10 , compared to a more accurate calculation, as we discuss in this paper. The usefulness of this ratio is that it allows simple predictions for the detectability in the GeV range based on the lower energy measurements. Here we discuss the validity of the simple analytical approximations, compared to more accurate numerical calculations of afterglow spectra at GeV energies.

In § 2 we describe the afterglow synchrotron-inverse Compton model used for the numerical computations, a comparison between numerical and analytical approximations being given in the Appendix. In § 3 we then present both numerical IC spectra and their appropriate analytical approximations, for the basic GRB afterglow model and for the extended models including new Swift-motivated elements such as injection or variable parameters, and evaluate their detectability as a function of redshift for the GLAST LAT instrument and for

AGILE.

2. Afterglow Synchrotron-inverse Compton Spectra at GeV Energies

The afterglow of a GRB, due to the external shock as it slows down in the external medium, produces synchrotron radiation in the X-ray to MeV range, which is then inverse-Compton upscattered into the GeV-TeV range (Mészáros et al. 1994; Böttcher & Dermer 1998). More specific calculation of the IC GeV range are, e.g. those of Sari & Esin (2001), Zhang & Mészáros (2001), Pe’er & Waxman (2004), etc. We describe the afterglow models, as usual, by the total isotropic energy $E_{52,iso} = E/10^{52}\text{erg}$ (for the case of energy injection see below), the external density n , a jet opening half-angle θ , electron equipartition parameter ϵ_e , magnetic equipartition parameter ϵ_B and electron energy index p . The other parameter of relevance in synchrotron-IC models is the scattering Y-parameter which is defined as the luminosity ratio of IC to synchrotron, usually given by

$$Y = (-1 + \sqrt{4\epsilon_e/\epsilon_B + 1})/2 . \quad (1)$$

The initial Lorentz factor Γ_0 of the burst is not needed as a parameter, since in the asymptotic blast wave regime the Lorentz factor follows from the scaling law,

$$\Gamma(t) = (17E/1024\pi nm_p c^5 t^3)^{1/8} \quad (2)$$

Our numerical calculations of the spectra and fluence curves use the basic synchrotron-IC equations given in Gou et al. (2006), extending now to the GeV range. We also consider in this range the spectral effects of the photon-photon opacity effects, which impose cutoffs depending on the spectrum and density of lower energy photons (Baring & Harding 1997; Lithwick & Sari 2001).

We calculate the synchrotron-IC spectra of three different types of GRB afterglow models, and evaluate their detectability with the GLAST Large Area Telescope (LAT) and with AGILE. These calculations improve on previous calculations, e.g. (Zhang & Mészáros 2001), in several respects. First, in the “standard” afterglow model such as used in (Zhang & Mészáros 2001), we use the exact IC spectrum instead of the broken power-law approximation, and the peak flux ratio is taken as F1 instead of F2 (see Appendix). Second, we include the complete spectral regimes, not only the commonly used $\nu_a < (\nu_m, \nu_c)$ regimes where ν_a , ν_m , and ν_c are the synchrotron self-absorption, injection, and cooling frequencies, respectively (Gou et al. 2006). This assures that the GRB afterglows evolve through the correct regimes at all times. Third, we consider Swift-motivated additions to the standard afterglow model,

such as a continued energy injection model, and a varying afterglow parameter model (motivated by the presence of a shallow decay phase, and a high apparent radiative efficiency, see e.g. Mészáros 2006 for a review).

The details of the three models calculated are as follows. (A) A standard afterglow model, with all parameters remaining constant during its evolution (for a detailed description of this model, see Gou et al. 2006). (B) A continuous energy injection model, which is a widely considered model to explain the shallow decay phase commonly seen in *Swift* light curves. For this, we assume that the total kinetic energy increases over time with a power-law index, $E \propto t^{1-q}$, before the break time $t = 10^4$ seconds and the break time here is defined as the one when the shallow decay phase ends. Fits to *Swift* observations indicate a value $q \sim 0.5$ (Zhang et al. 2006). (C) An evolving parameter model, which is an alternative model for explaining the shallow decay phase, based on the assumption that the electron equipartition parameter ϵ_e increases with the time as $\propto t^\alpha$ (Ioka et al. 2006) before the break time, as for the energy injection model. For all three models, we assume that they have the same parameters at late times, i.e. after the break time. Since the flux has to be integrated over the observation time, we set the observation time to be one half of the final time of observation since the trigger (e.g. if the observational data stop at $t = 10^5$ seconds, the integration time is from $t = 5 \times 10^4$ seconds to $t = 10^5$ seconds). This is consistent with the GLAST observation characteristics, as well as those of AGILE, in the point-source observing mode, where due to earth occultation, only about 50% of the orbit time is used for the burst observation.

To determine the limiting redshift to which a burst can be detected, we calculate the instrumental fluence threshold as in Zhang & Mészáros (2001), using the instrument characteristics of the GLAST LAT and AGILE. For a flux sensitivity Φ_m ph cm⁻² s⁻¹ over an exposure time T and a point source observed over an effective observation time t_{eff} (in seconds) in an energy band centered around a photon energy E , the fluence threshold is estimated as $F_{thr} \sim [\Phi_o(T/t_{eff})^{1/2}]Et_{eff}$ where $[\Phi_o(T/t_{eff})^{1/2}]$ is the sensitivity for the effective observation time t_{eff} because the sensitivity scales as $\sqrt{t_{eff}}$ for the longer observations where the sensitivity is limited by the background. Due to the occultation by the earth, the effective observation time t_{eff} is normally $\leq 50\%$ of the total orbit time, t_{obs} , for both GLAST and AGILE (or equivalent to the observation time after the burst), namely, $t_{eff} = \eta t_{obs}$ where the observing efficiency η is taken to be $\eta = 0.5$. Hereafter, unless otherwise stated, the small “t” without the subscript refers to the observation time t_{obs} for simplicity. For GLAST we use the fluence threshold listed in the updated instrument performance documents². Consid-

² http://www-glast.slac.stanford.edu/software/IS/glast_lat_performance.htm

er the integral sensitivity above 100 MeV for GLAST LAT to be $\sim 4 \times 10^{-9} \text{ ph cm}^{-2} \text{ s}^{-1}$ for an effective observation time of one year in the sky-survey mode, the fluence threshold is $1.0 \times 10^{-8} t^{1/2} \text{ erg cm}^{-2}$ for the long-time observation in the sky-survey mode. For GRB afterglows, in most cases GLAST will perform a pointed observation rather than the survey mode observation. In this mode, GLAST will keep the GRB position always at the center of the LAT field of view for as long as possible, and this will improve the sensitivity by a factor of 3-5 (depending on where the GRB lies with respect to the orbital plane; an object which lies at the orbit pole will not be occulted by the Earth and can be continuously observed; J. McEnery 2007, private communication). Therefore, taking the improvement factor of 3, the fluence threshold for a GRB observation is $3.4 \times 10^{-9} t^{1/2} \text{ erg cm}^{-2}$ for the long-time observation. The short-time fluence threshold can be defined by the criterion that at least 5 photons are collected and it depends on the effective area of the instrument which is around 6000 cm^2 at 400 MeV for GLAST LAT, so it is $5.3 \times 10^{-7} \text{ erg cm}^{-2}$ (the transition time when the short-time sensitivity and long-time sensitivity meet is 2.4×10^4 seconds). Compared to the previous estimate of Zhang & Mészáros (2001) for the GLAST sensitivity, the short-time observation sensitivity here is roughly the same, but the long-time sensitivity has changed from $1.2 \times 10^{-9} t^{1/2}$ to $3.4 \times 10^{-9} t^{1/2} \text{ erg cm}^{-2}$, increased by a factor of 3.

The energy range of AGILE is somewhat lower than that of GLAST LAT. Its flux sensitivity above 100 MeV is $\sim 3 \times 10^{-7} \text{ ph cm}^{-2} \text{ s}^{-1}$ for a point-source observation over an effective period of 10^6 seconds (Tavani et al. 2006). Thus, taking the observing efficiency $\eta = 0.5$, the fluence threshold can be estimated as $3.0 \times 10^{-7} (T/t_{eff})^{1/2} E t_{eff} \approx 1.3 \times 10^{-7} t^{1/2} \text{ ergs cm}^{-2}$ at an average energy of 400 MeV, where $T = 10^6$ seconds is the exposure time corresponding to the given sensitivity. The fluence threshold is for the long-time observation. The shorter-time fluence threshold can be obtained similarly as above, $\sim (5/550) \times 400 \text{ MeV} \sim 5.8 \times 10^{-6} \text{ ergs cm}^{-2}$ where we have taken the effective area for AGILE to be 550 cm^2 . In summary, for AGILE, the fluence threshold for the long-time observation (i.e., $t > 1870$ seconds) is $1.3 \times 10^{-7} t^{1/2} \text{ ergs cm}^{-2}$ and $5.8 \times 10^{-6} \text{ ergs cm}^{-2}$ for the short-time observation, the transition time being $\simeq 1870$ seconds.

3. Detectability of GRB Afterglows with GLAST and AGILE

The initial nominal set of parameters for the standard model (A) used here are the same as for the standard model of Zhang & Mészáros (2001): $p = 2.2$, $\epsilon_e = 0.5$, $\epsilon_B = 0.01$, $E_{52,iso} = 1$, $n = 1 \text{ cm}^{-3}$. An additional feature is that we also assume a jet opening half-angle $\theta = 0.14$, which does not affect the flux at early times. The other parameters are as for model (A). For the injection model (B), the kinetic energy is assumed to increase following the relation

$E \propto t^{1-q} = t^{0.5}$ where q is taken to be 0.5 based on the *Swift* observation fits (Zhang et al. 2006). For the model (C) with evolving parameters, we assumed ϵ_e to follow the relation $\epsilon_e \propto t^{0.5}$ (Ioka et al. 2006), other parameters being the same as for model (A). In the alternative models (B) and (C), either the kinetic energy or the electron equipartition parameter starts out with a smaller value as for (A), but at late times end up with the same values as the standard model (A). The transition time at which the energy injection or the ϵ_e evolution stops is set at $t = 10^4$ seconds.

Fig 1 shows the results for the three models above, using the nominal set of parameters. Panel (a) shows the partial fluence, defined here as the energy flux integrated over the time intervals $[t - \Delta t, t]$, as a function of t , where the $t = t_{obs}$ is the observation time counted after the trigger, adopting a nominal integration time $\Delta t = 0.5t$ throughout. The partial fluence curves shown correspond to the three different GRB afterglow models, (A) the standard model, which is the same as the type II GRB model in Zhang & Mészáros (2001); (B) the energy injection model; (C) the evolving parameter model. As can be seen in panel (a), for a burst at a low redshift $z = 0.32$ the GeV emission from all three models can be detected by GLAST up to a time $t \sim 1.5 \times 10^5$ seconds. Note that the GeV emission from the standard model is higher than that from the two other models. This is because all the models end up with the same energy and same parameters at late times, which means the injection starts with lower energy and the evolving parameter begins with the lower ϵ_e at the beginning. Panel (b) shows the synchrotron and IC spectra of the standard model (A) at times $t = 10^2, 10^3, 10^4, 10^5$, and 10^6 seconds. Hereafter, unless otherwise stated, we always calculate the spectra at these time epoches. The fluxes around TeV (10^{12} eV) show the effects of including photon-photon absorption within the sources. The upper curves are the flux without the $\gamma\gamma$ absorption, and the lower curves are the flux after internal absorption. For this we have used the optical depth of to internal $\gamma\gamma$ interactions of Equation (20) in Zhang & Mészáros (2001). For the relatively low compactness parameters of the external afterglow shock discussed here, the $\gamma\gamma$ cutoff becomes important above \sim TeV energies, which is more of interest for ground-based air Cherenkov telescope observations than for space detectors. The lower panels (c) and (d) show the redshift dependence of the GeV emission for all three models, at $t \sim 1.1 \times 10^3$ and $t \sim 2 \times 10^4$ seconds. At $t \sim 1.1 \times 10^3$ seconds, the limiting redshift is $z \sim 0.4$ for the standard model and $z \sim 0.22$ for other two models. At $t \sim 2 \times 10^4$, the limiting redshift is around $z \sim 0.45$ for all the models.

Note that while the usual fluence is defined as flux integrated over the observation time since the trigger, which always increase with time, the partial fluences shown in panel (a) first increase and eventually decrease. This is because the afterglow flux decreases with time t , and for the partial fluences the integration time starts at $0.5t$ and ends at t . This is done to check the limiting redshift to which afterglows can be detected for typical observations

at different epochs t with some uniform criterion for the integration time. The snapshot at the time 2×10^4 seconds lies where the partial fluence is roughly flat in time, during which period the limiting redshift reaches its maximum (although the partial fluence within the flat phase varies by a factor ≤ 2 , the limiting redshift changes only slightly). Other snapshot epochs were chosen around one decade earlier or later than the typical maximum redshift epoch.

In Fig 2 we consider an alternative set of parameters. The motivation for this is that the parameters of the standard model shown in Figure 1, $E_{52,iso} = 1$, $\epsilon_e = 0.5$, differ somewhat from the ‘statistical average’ values quoted for low-redshift GRBs, $E_{52,jet} \sim 0.1$ and $\epsilon_e \sim 0.1$, e.g. Panaitescu & Kumar (2001). In order to check the sensitivity of the detectability of GRBs to variations in these parameters, we performed the same calculation using the values $p = 2.2$, $\epsilon_e = 0.2$, $\epsilon_B = 0.01$, $E_{52,iso} = 10$, $n = 1 \text{ cm}^{-3}$, $\theta = 0.14$, the results being shown in Fig (2). For these ‘average’ parameters, the limiting redshift is $z \simeq 0.8$ for all three GRB models.

In Fig 3 we show the corresponding results for AGILE. This is a smaller-scale mission than GLAST, launched in April 23, 2007, and it is interesting to compare its detectability limits with those of GLAST. AGILE has a different energy range (30 MeV to 50 GeV) and has a relatively narrower energy band than that of the GLAST LAT (20 MeV to 300 GeV), as well as a lower effective area. Thus the observed fluxes and partial fluences are expected to be lower for AGILE in contrast to GLAST. This is seen in Panel (a) of Fig 3. The dashed line is for AGILE, and the solid line is for GLAST), showing that it is hard for AGILE to detect a burst with the typical parameters at $z = 0.32$, while GLAST could detect it until around 2 days. Panels (b), (c) and (d) of Fig 3 show the detectability with AGILE and with GLAST at different time epochs. At $t = 1.1 \times 10^3$ seconds, AGILE can detect bursts up to $z \simeq 0.25$, and GLAST can detect bursts to $z \simeq 0.8$. At the time $t = 2.0 \times 10^4$ seconds, the limiting redshifts are 0.15 for AGILE, and 0.8 for GLAST (same as Fig 2), respectively. At $t = 1.4 \times 10^5$ seconds, the limiting redshift for AGILE is apparently well below $z = 0.1$, while the limiting redshift for GLAST can still reach up to 0.5. We see that the limiting redshift for AGILE drops relatively quickly with increasing observation times; the short-time sensitivity for AGILE lasts around 10^3 seconds, and after that the sensitivity drops quickly. For GLAST, the short-time sensitivity lasts a longer time, $\sim 10^4$ seconds, and since the afterglow GeV flux doesn’t change much for up to one day after the trigger, we don’t expect the sensitivity drop to have much of an effect on the limiting redshift for GLAST.

In Figure 4 we probe the sensitivity of the detectability on the total kinetic energy of the burst, taking as an example the results for a value of $E_{52,iso} = 100$. This is in the range of values derived for objects such as GRB 990123 and GRB 050904, which may be called

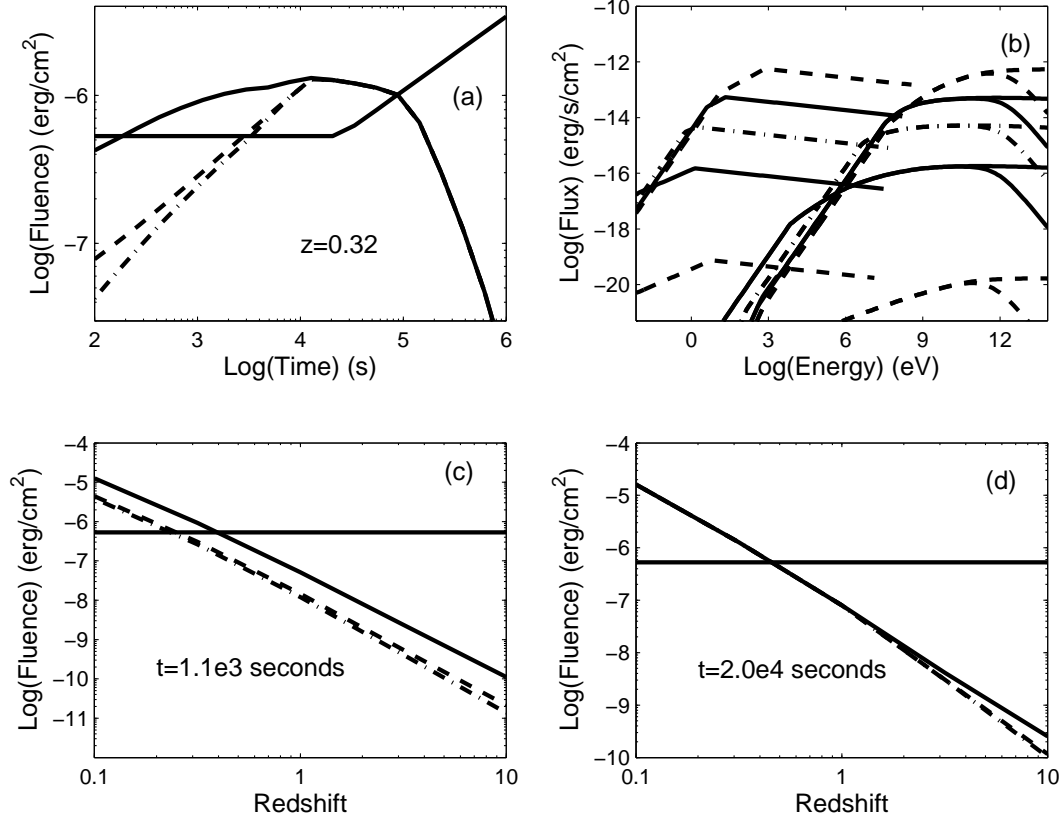


Fig. 1.— *Panel (a)* The partial fluence curves (defined as flux integrated between $0.5t$ and t) as a function of the observation time t since the trigger, for the three GRB afterglow models in the GLAST LAT energy band, at a redshift $z = 0.32$. Solid curves: standard model (A) (constant energy); dashed curves: “energy injection” model (B); dot-dashed curves: “evolving parameter” model (C). The sensitivity of the GLAST LAT is shown by the broken solid curve. The parameters for the standard model are $E_{52,iso} = 1$, $\epsilon_e = 0.5$, $\epsilon_B = 0.01$, $p = 2.2$, $\theta = 0.14$ and the break time when the shallow decay phase ends is at $t = 10^4$ seconds. Before the break time, $\epsilon_e \propto t^{0.5}$ in the evolving parameter model, and the kinetic energy $E \propto t^{0.5}$ in the energy injection model. After the break time, those parameters will be the same as the ones in the standard model. *Panel (b)* The synchrotron and IC spectrum for the standard model at different time epochs: 10^2 , 10^3 , 10^4 , 10^5 , and 10^6 seconds, respectively. Above photon energies $\sim 10^{12}$ eV, the upper spectral curve represents the flux without γ - γ absorption, and the lower curve is with inclusion of this absorption. *Panel (c)* The redshift dependence of the partial fluence for the three models above, evaluated at the observation time $t \sim 1.1 \times 10^3$ seconds. The solid line is the GLAST sensitivity for an integration time 550 seconds (the observing efficiency 0.5 has been taken). The intersection of the partial fluence and the sensitivity curve gives the limiting redshift, to which the bursts can be detected by GLAST for this integration time, which is $z \simeq 0.4$ for the standard model, and $z \simeq 0.22$ for the other two models. *Panel (d)* The redshift dependence of the partial fluence for the three models above, evaluated at $t \sim 2.0 \times 10^4$ seconds. The solid line is the GLAST sensitivity for an integration time 10^4 seconds. The intersection gives a limiting redshift for detection of $z \simeq 0.45$ for all three models.

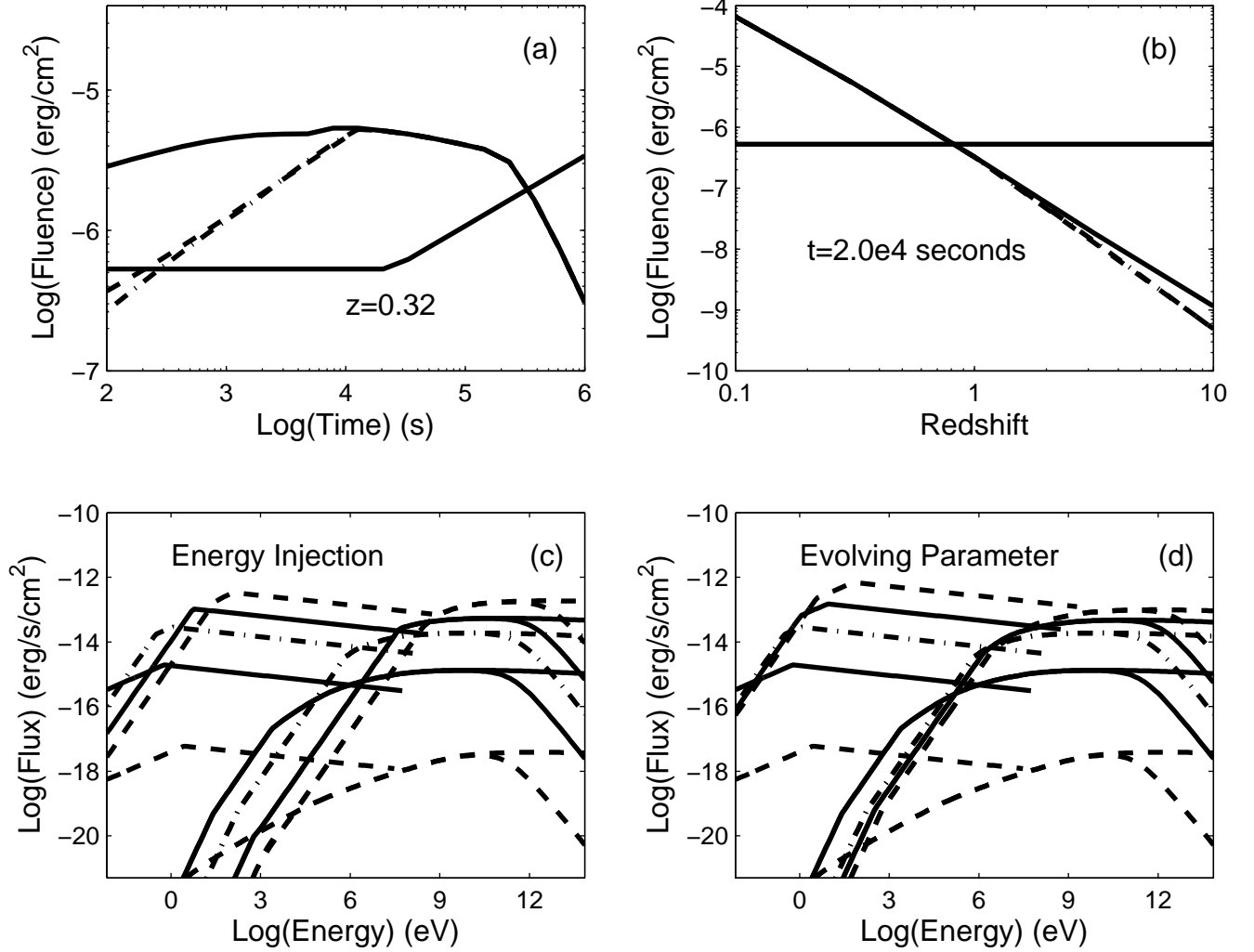


Fig. 2.— *Panel (a)* The partial fluence curves of the same three GRB afterglow models over the GLAST energy band, for a different set of parameters generally assumed to be 'typical', namely kinetic energy $E_{52,iso} = 10$, $\epsilon_e = 0.2$ and other parameters the same as in Fig (1). *Panel (b)* The redshift dependence of the partial fluence at $t = 2 \times 10^4$ s for the same models, giving a limiting redshift $z \simeq 0.8$. *Panel (c)* The synchrotron-IC spectra for the energy injection case. *Panel (d)* The synchrotron-IC spectra for the evolving parameter case.

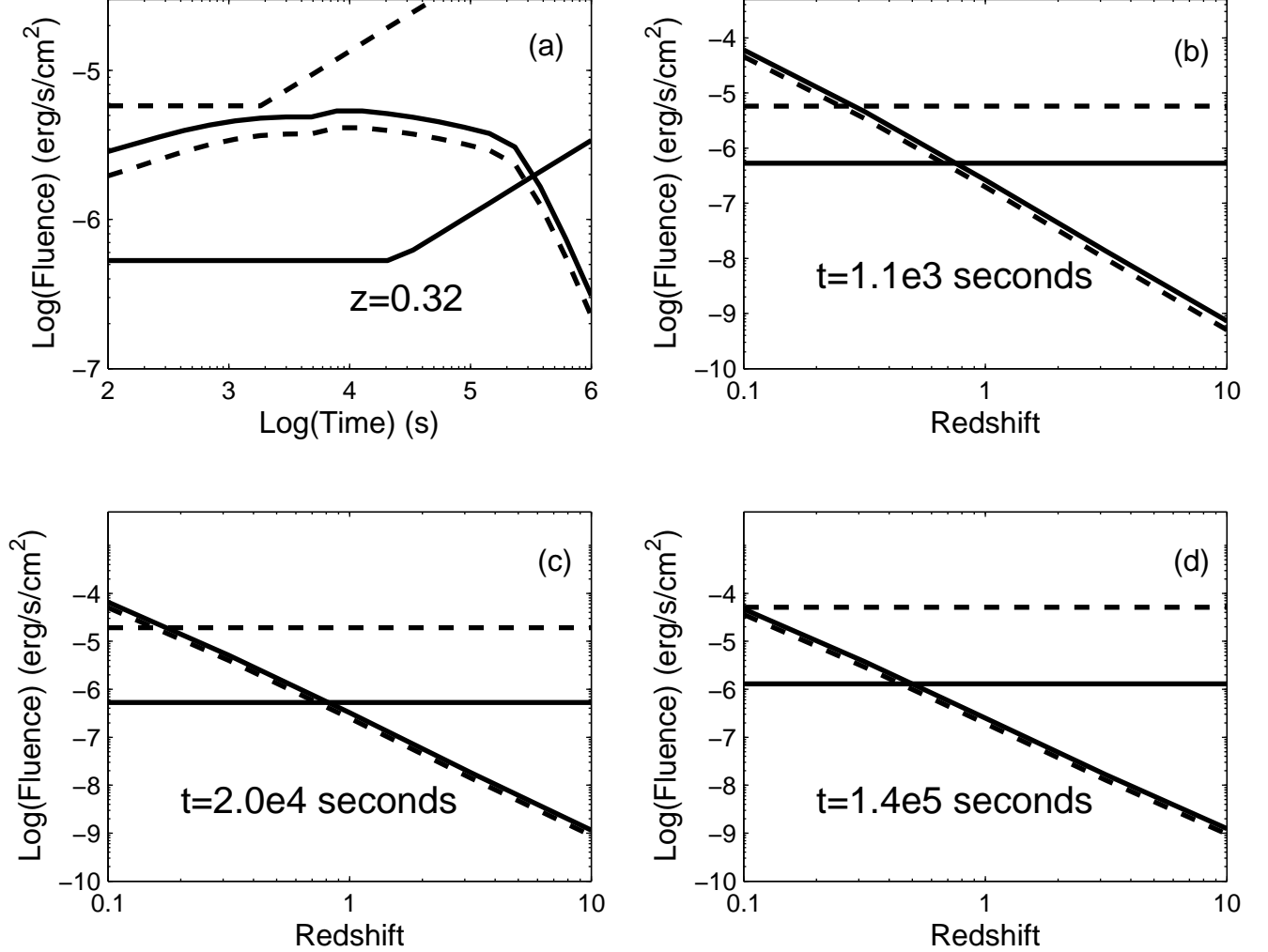


Fig. 3.— Comparison of GLAST and AGILE detectability. *Panel (a)* The partial fluence curves for the standard model over the energy bands of AGILE (dashed lines) and GLAST (solid lines), compared to the respective instrument sensitivities. The parameters are the same as in Fig 2. *Panel (b)* The redshift dependence of the partial fluence at $t = 1.1e4$ seconds. The limiting redshifts are $z = 0.25$ for AGILE, and $z = 0.8$ for GLAST, respectively. *Panel (c)* The redshift dependence of the partial fluence at $t = 2.0 \times 10^4$ seconds. The limiting redshift points are $z = 0.15$ for AGILE, and $z = 0.72$ for GLAST, respectively. *Panel (d)* The redshift dependence of the partial fluence at $t = 1.4 \times 10^5$ seconds. The limiting redshift for AGILE is below $z \sim 0.1$, and the limiting redshift for GLAST is around $z = 0.5$, for this model.

hyper-energetic GRB. For the “standard” model case (A) with this energy (see upper panel of Fig 4) we see that the limiting redshift for a GLAST detection has increased from $z \simeq 0.8$ to a value $z \simeq 2.0$, assuming that the other parameters remain the same as in Figure 2. Thus, hyper-energetic bursts such as GRB 990123, at the observed redshift $z = 1.6$, should be detected by GLAST in the GeV band, if they have the above conventional parameters. The other hyper-energetic object, GRB 050904, has a similar kinetic energy as GRB 990123, but it was at the much higher redshift $z = 6.29$, which appears out of range for GLAST. GRB 050904 had the most complete set of observational data so far, covering from the BAT band, through X-ray, to the optical/NIR and to the radio band. Thus a lot of effort has been invested in obtaining the best fitting parameters for this burst (Frail et al. 2006; Gou et al. 2006). Taking the best fitting parameters from model (B) of Gou et al. (2006), our results here indicate that such GRB 050904-like bursts could be detected by GLAST up to $z \leq 1.0$. There are two reasons for this relatively modest limiting redshift detectability by GLAST in this case: (1) The electron equipartition parameter derived is small, $\epsilon_e = 0.026$, which means only a fraction of the kinetic energy is radiated; (2) The Compton parameter in the fast cooling case is relatively small, $Y \simeq 1.7$, which means that the energy lost via IC scattering is comparable to the energy lost via synchrotron radiation.

In Figure 5 we illustrate the sensitivity of the GeV detectability on the value of the Compton Y parameter, showing the fluxes for two values, $Y = 2.7$ (solid line) and $Y = 6.6$ (dashed line) in the fast cooling case. The parameters are same as the ones of the standard case (A) in Fig. 2, except for the electron equipartition parameter ϵ_e , which is $\epsilon_e = 0.1$ for the $Y = 2.7$ case and $\epsilon_e = 0.5$ for the $Y = 6.6$ case. One expects a higher flux over the GLAST energy band for the $Y = 6.6$ case because a larger Compton parameter means that more energy goes into the GeV band via the IC process, which can be seen from the spectrum on the lower panels. The limiting redshifts for observation times $t = 2.0 \times 10^4$ seconds are $z = 0.55$ and $z = 1.2$, respectively, for $Y = 2.7$ and $Y = 6.6$.

4. Discussion

We have calculated the time-dependent GeV synchrotron and inverse Compton spectra for three generic types of GRB afterglows which, at lower photon energies, have been used to interpret observations from the Swift satellite and other ground-based facilities. These models include a standard, constant parameter afterglow model (A), a model with late injection (B) and a model with varying parameters (C). The spectra and the GeV partial fluence curves in the GeV range were used to estimate the detectability with GLAST and AGILE of bursts in these model categories, for various sets of parameters, at various epochs

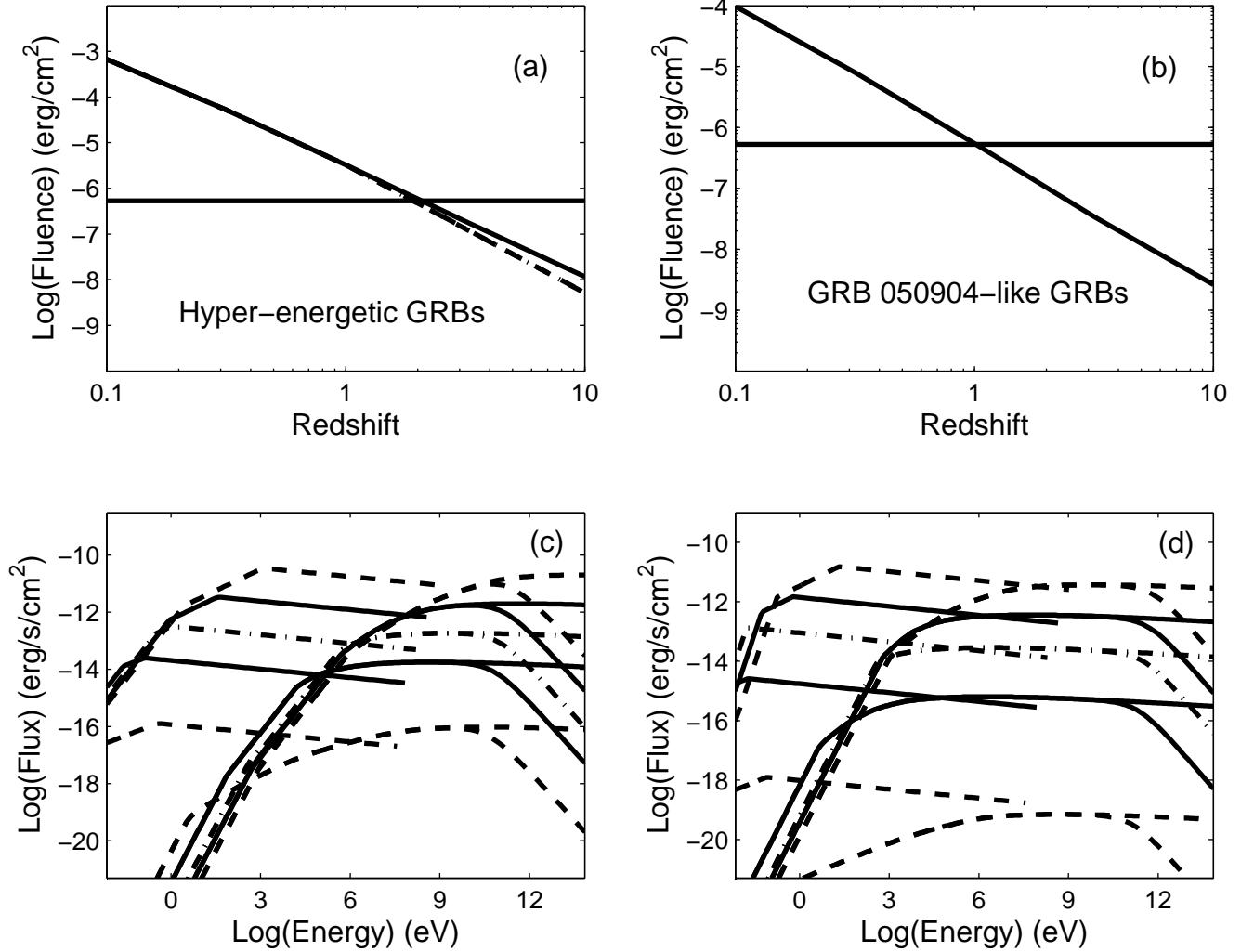


Fig. 4.— Standard models of type (A), with different values of the parameters. *Panel (a)* The redshift dependence of the GeV partial fluence for hyper-energetic GRB 990123-like objects, at $t = 2.0 \times 10^4$ seconds. The intersection point gives the limiting redshift $z \simeq 2$ below which GLAST can detect such afterglows in the GeV band. The model parameters are $E_{52,iso} = 100$, $\epsilon_e = 0.2$ and the other parameters are the same as in Fig (1). *Panel (b)*: The redshift dependence of the partial fluence for model (B) of GRB 050904 using the best fitting for this bursts parameters (Gou et al. 2006), $p = 2.194$, $\epsilon_e = 0.026$, $\epsilon_B = 0.0058$, $n = 109$, $\theta = 0.111$, $E_{52,iso} = 184.8$, at the time $t = 2.0 \times 10^4$ seconds. The limiting redshift for such GRB 050904-like objects is $z \simeq 1$. *Panel (c)* The synchrotron and IC spectrum for hyper-energetic GRB 990123-like objects. *Panel (d)* The synchrotron and IC spectrum for GRB 050904-like GRBs.

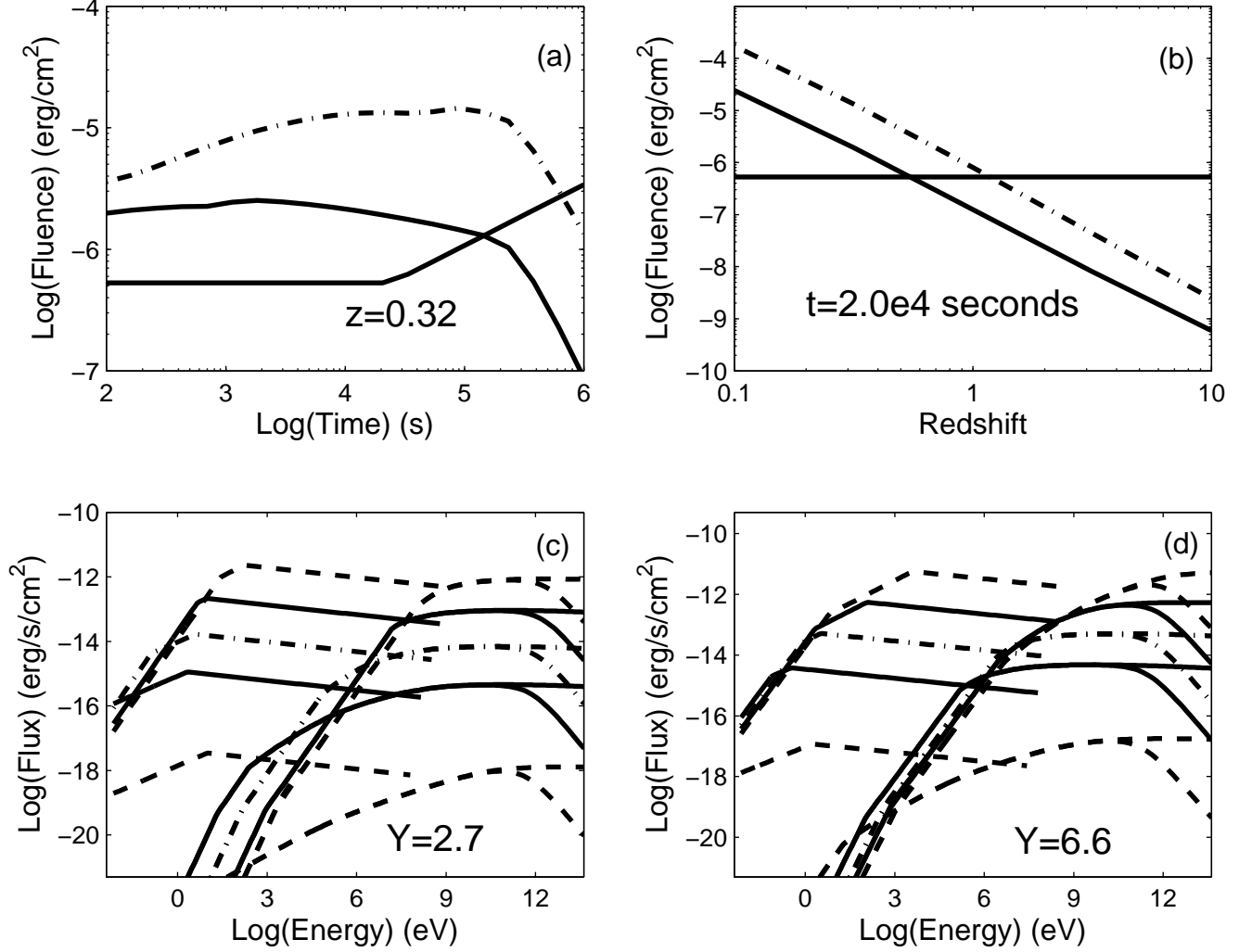


Fig. 5.— Detectability limits for GLAST for standard models such as (A) but with different Compton Y parameters, $Y = 2.7$ and $Y = 6.6$. *Panel (a)* The partial fluence curves for $Y = 6.6$ (dashed dotted line) and $Y = 2.7$ (solid line), compared to the GLAST sensitivity (solid broken line). *Panel (b)* The limiting redshift for an observation time $t = 2 \times 10^4$ s and the two Y parameters, giving limiting redshifts $z = 0.55$, and $z = 1.2$, respectively. *Panel (c)* The synchrotron and IC spectra for the Compton parameter $Y = 2.7$ case. *Panel (d)* The synchrotron and IC spectra for the Compton parameter $Y = 6.6$ case.

after the trigger and for various observation durations. These model spectra improve on previous calculations in several respects. In particular, in the past mainly constant parameter spectral models such as (A) were computed; here we have extended these calculations over a broader range of input parameters, based on more recent information and statistics. Models (B) and (C) have not been previously investigated in the GeV range, and are motivated by recent Swift results. The GeV spectra discussed here were computed numerically, using the formalism described in Gou et al. (2006). These are compared with previous analytical synchrotron-inverse Compton spectra of type (A) in the appendix.

The detectability depends most obviously on the total burst energy $E_{52,iso}$ and on the observation time t and integration time Δt , in addition to the other parameters such as ϵ_e , ϵ_B etc. E.g., for bursts of the standard constant parameters (A) with the nominal values of the parameters $E_{52,iso} = 1$, $\epsilon_e = 0.5$, $\epsilon_B = 0.01$, the limiting detection redshift with GLAST for times $t = 1.1 \times 10^3$ s and 2×10^4 s and integration time $\Delta t = 0.5t$ are roughly the same, $z \simeq 0.4$ (Fig. 1, panel b and c). For models with energy injection (B) or varying parameters (C), where the final values of E_{iso} or ϵ_e reach the same value as for model (A) at a later time, the detection threshold is somewhat lower for the shorter observation time, as seen in the same figure, panel c, since they start out weaker and build up to be comparable to (A) at later times. However, for the longer of the two observation times above, panel d, the limiting redshifts are the same. For the more standard values $E_{52,iso} = 10$, $\epsilon_e = 0.2$ (Fig. 2, panel b) the limiting redshift for the constant parameter model (A) at $t = 2 \times 10^4$ s goes up to $z \simeq 0.8$.

For AGILE the limiting redshifts are lower than for GLAST due to its lower effective area. For a standard burst model (A) with average parameter values $E_{52,iso} = 10$, $\epsilon_e = 0.2$, the limiting redshift is $z \simeq 0.25$ at an earlier observation time $t = 1.1 \times 10^3$ s (Fig. 3, panel b), and $z \simeq 0.15$ at $t = 2 \times 10^4$ s. With AGILE bursts can only be detected at relatively early times, since the short-time sensitivity for AGILE (where the sensitivity curve is flat in time) only lasts, e.g. around $\sim 10^3$ seconds, versus $\sim 10^4$ s for GLAST for a burst at $z \sim 0.3$ (Fig. 3, panel a).

A discrimination between models (A), (B) and (C) based on GeV measurements of the spectral evolution in time is possible in principle, as seen e.g. by comparing Fig. 1 panel (c), and Fig. 2 panels (c) and (d). However, it will require good energy and time coverage, and extensive simulations over a wide range of parameter space, since changes in E_{iso} , Y (e.g. Figs. 4 and 5) and the other afterglow parameters needs to be carefully disentangled.

The limiting redshift naturally increases for larger values of E_{iso} . E.g., for GLAST at an observation time $t = 2 \times 10^4$ s and a standard model (A) with $E_{52,iso} = 10^2$, $\epsilon_e = 0.2$ it is $z \simeq 2$, while for a burst with the parameters of GRB 050904 (high E_{iso} but low ϵ_e) it is

$z \simeq 1$. The limiting redshift also increases with the Compton Y parameter, as illustrated in Fig. 5, which reflects the fact that Y provides a measure of how much energy gets scattered into the GeV range.

The detectability estimates discussed here illustrate the sensitivity to different types of model assumptions in current synchrotron-inverse Compton models, when one takes into account newer information gleaned from *Swift*. Calculations using simplified generic models show that around tens of *Swift*-detected GRB per year will fall in the LAT field of view (Omodei & The GLAST/LAT GRB Science Group 2006) during their prompt emission phase. Considering the *Swift*-detected burst redshift distribution to imply a fraction of around 20% below $z = 1$ (Jakobsson et al. 2006; Le & Dermer 2006), we may roughly expect ~ 5 *Swift*-burst prompt detections per year by GLAST. However, since the GeV afterglows can last up to a day (e.g. Figs. 1 and 2, panel a), GLAST may actually be able to observe more than this number of bursts in the afterglow, as opposed to the prompt phase. Detections with GLAST should test many of the assumptions that go into these models, and will provide important new information on the energetics, dynamics and parameters of GRB afterglows.

We are grateful to J. McEnery for informative correspondence, and D. Fox, X.Y. Wang, and B. Zhang for useful comments. This research has been supported in part through NASA NAG5-13286 and NSF AST 0307376. L. J. Gou also thanks support from a Sigma-Xi Fellowship.

REFERENCES

- Baring, M. G. & Harding, A. K. 1997, ApJ, 491, 663
- Böttcher, M. & Dermer, C. D. 1998, ApJ, 499, L131+
- Chiang, J. & Dermer, C. D. 1999, ApJ, 512, 699
- Fan, Y.-Z. et al. 2007, ArXiv e-prints, arXiv:0704.2063
- Fox, D. B. & Mészáros, P. 2006, New Journal of Physics, 8, 199
- Fragile, P. C. et al. 2004, Astroparticle Physics, 20, 591
- Frail, D. A. et al. 2006, ApJ, 646, L99
- Gou, L. J., Fox, D. B., & Mészáros, P. 2006, ApJ submitted, astro-ph/0612256

- Gupta, N. & Zhang, B. 2007, ArXiv e-prints, arXiv:0704.1329
- Ioka, K. et al. 2006, A&A, 458, 7
- Jakobsson, P. et al. 2006, A&A, 447, 897
- Kobayashi, S. et al. 2007, ApJ, 655, 391
- Le, T. & Dermer, C. D. 2006, ArXiv Astrophysics e-prints
- Lithwick, Y. & Sari, R. 2001, ApJ, 555, 540
- McEnery, J. & GLAST Mission Team 2006, in American Institute of Physics Conference Series, Vol. 836, Gamma-Ray Bursts in the Swift Era, ed. S. S. Holt, N. Gehrels, & J. A. Nousek, 660–663
- Mészáros, P. 2006, Reports of Progress in Physics, 69, 2259
- Mészáros, P., Rees, M. J., & Papathanassiou, H. 1994, ApJ, 432, 181
- Nousek, J. A. et al. 2006, ApJ, 642, 389
- Omodei, N. & The GLAST/LAT GRB Science Group 2006, in American Institute of Physics Conference Series, Vol. 836, Gamma-Ray Bursts in the Swift Era, ed. S. S. Holt, N. Gehrels, & J. A. Nousek, 642–647
- Panaitescu, A. & Kumar, P. 2000, ApJ, 543, 66
- 2001, ApJ, 560, L49
- Panaitescu, A. & Mészáros, P. 1998, ApJ, 501, 772
- Pe’er, A. & Waxman, E. 2004, ApJ, 603, L1
- Rybicki, G. B. & Lightman, A. P. 1979, Radiative processes in astrophysics (New York, Wiley-Interscience, 1979. 393 p.)
- Sari, R. & Esin, A. A. 2001, ApJ, 548, 787
- Tavani, M. et al. 2006, in Presented at the Society of Photo-Optical Instrumentation Engineers (SPIE) Conference, Vol. 6266, Space Telescopes and Instrumentation II: Ultraviolet to Gamma Ray. Edited by Turner, Martin J. L.; Hasinger, Günther. Proceedings of the SPIE, Volume 6266, pp. 626603 (2006)., ed. M. J. L. Turner & G. Hasinger
- Totani, T. 1998, ApJ, 502, L13+

Wang, X. Y., Dai, Z. G., & Lu, T. 2001, ApJ, 556, 1010

Wang, X.-Y., Li, Z., & Mészáros, P. 2006, ApJ, 641, L89

Wei, D. M. & Lu, T. 1998, ApJ, 505, 252

Zhang, B. 2007, Chinese Journal of Astronomy and Astrophysics, 7, 1

Zhang, B. et al. 2006, ApJ, 642, 354

Zhang, B. & Mészáros, P. 2001, ApJ, 559, 110

5. Appendix

We discuss here two analytical approximations to the synchrotron-IC spectrum, and compare them to the numerically calculated values. The two key elements in the simple analytical approximations to synchrotron-IC spectra in the literature are (i) an IC to synchrotron peak flux ratio,

$$F \equiv f_{max}^{IC} / f_{max}^{syn} \quad (3)$$

expressed, e.g. in $\text{erg cm}^{-2} \text{s}^{-1} \text{Hz}^{-1}$ and evaluated at the frequencies where the synchrotron and the IC flux attain their peak value, and (ii) a “Compton parameter” Y , usually taken to be

$$Y = (-1 + \sqrt{4\epsilon_e/\epsilon_B + 1})/2 . \quad (4)$$

In the GRB literature, the flux ratio (3) of the analytical approximations has appeared under several forms, two of which are the most relevant for us here. One of these is

$$F1 \equiv f_{max}^{IC} / f_{max}^{syn} = (14/45)\sigma_T R n \simeq \tau \quad (5)$$

(see Sari & Esin 2001, A9), where σ_T is the Thompson scattering cross section, R is the shock radius, n is the external circumburst density in units of cm^{-3} , and $\tau = \sigma_T R n / 3$ is the Thompson optical depth of the radiation region³. Another form of this ratio which has been used is

$$F2 \equiv f_{max}^{IC} / f_{max}^{syn} = [4(p-1)/(p-2)]\tau , \quad (6)$$

This preprint was prepared with the AAS L^AT_EX macros v5.2.

³The optical depth here differs from the usual definition by a factor 1/3, but for consistency with the usage in the literature (Panaitescu & Kumar 2000; Kobayashi et al. 2007) we keep the factor 1/3 here.

(Kobayashi et al. 2007). It is apparent that F1 is smaller than F2 by a factor $[4(p-1)/(p-2)]$, which can give substantial differences in analytical estimates of the IC spectral flux at its peak. It is worthwhile therefore to clarify the reason for the discrepancy.

The F1 form (equation [5]) of the peak flux ratio is derived from an integral over the electron energy distribution and a power-law seed synchrotron spectrum (See Eqn. (7.28), Rybicki & Lightman 1979; Also Eqn. (A1), Sari & Esin 2001).

The F2 form (equation [6]) of the peak flux ratio, on the other hand, is obtained by solving for $f_{max}^{IC}/f_{max}^{syn}$ from an equation (7) which relates the Compton Y parameter to the ratio of the luminosities produced by the first order IC and the synchrotron mechanisms (Kobayashi et al. 2007),

$$Y = L_{IC,1st}/L_{syn} \sim \nu_{peak}^{IC} f_{\nu}^{IC}(\nu_{peak}^{IC}) / \nu_{peak} f_{\nu}(\nu_{peak}) = 2\kappa\tau\gamma_m\gamma_c \quad (7)$$

where ν_{peak}^{IC} and ν_{peak} are the peak frequency of the inverse Compton and synchrotron spectra, respectively, and $f_{\nu}^{IC}(\nu_{peak}^{IC})$ and $f_{\nu}(\nu_{peak})$ are the peak fluxes corresponding to the IC and synchrotron peak frequencies. The corresponding analytical approximation to the IC spectrum is a simpler one than in the previous F1 case, in that it is a broken power law (without the logarithmic corrections). In the low-frequency part of the IC spectrum, the broken power law is a good approximation to a numerically calculated IC spectrum. However, in the high-frequency part, the broken power-law analytical approximation under-estimates the numerical IC spectrum, which is larger (and has a flatter spectral index) than the broken power-law prediction (this under-estimation is avoided in the F1 case by including the logarithmic correction). In the F2 pure broken power law case, therefore, in order to keep the frequency integrated total luminosity radiated by the IC mechanism equal to the numerically computed total IC luminosity, and to preserve the desirable simple broken power law shape, an artificially boosted peak flux ratio is adopted, which leads to the same total IC to synchrotron luminosity ratio. Thus, while the total energetics are the same for both analytical approximations, the IC flux expected over the GLAST (and AGILE) energy range differ. Whereas F2 is simpler for quick estimates since it involves pure power laws and correctly describes the global energetics, F1 with the logarithmic corrections to the power laws is preferable for more accurate GeV spectral flux estimates.